Journal of Clinical and Translational Hepatology **2026**
DOI: 10.14218/JCTH.2026.00312

Original Article

Lipid Metabolism-related lncRNA Model Identifies *AC026412.3* as a Driver of Fatty Acid β-oxidation in Hepatocellular Carcinoma

Lixin Liu[1#], Yuhao Fan[2#], Hao Zou[1], Sheng Hu[1], Kui Long[1], Lianghua Li[1], Chaosheng Xia[1], Hongyue Wang[1], Yang Liu[1], Runlin Feng[3], Zongqi Deng[4*] and Qiang Kang[1*]

[1]Department of Hepatopancreatobiliary Surgery, The Second Affiliated Hospital of Kunming Medical University, Kunming, Yunnan, China; [2]Department of Gastrointestinal Surgery, The Second Affiliated Hospital of Kunming Medical University, Kunming, Yunnan, China; [3]Department of Pathology, The Second Affiliated Hospital of Kunming Medical University, Kunming, Yunnan, China; [4]The Second Affiliated Hospital of Kunming Medical University, Kunming, Yunnan, China

Received: April 30, 2026 | **Revised:** July 01, 2026 | **Accepted:** July 16, 2026 | **Published online:** August 13, 2026

Abstract

Background and Aims: Dysregulated lipid metabolism contributes to hepatocellular carcinoma (HCC) progression, but the prognostic value and mechanistic roles of lipid metabolism-related long noncoding RNAs (LRLs) remain insufficiently characterized. This study aimed to construct and validate an LRL-based prognostic model and to investigate the biological function and metabolic mechanism of *AC026412.3* in HCC. ***Methods:*** Transcriptomic and clinical data from the The Cancer Genome Atlas Liver Hepatocellular Carcinoma cohort were analyzed to identify LRLs based on their correlation with curated lipid metabolism genes. Differential expression, univariate Cox, least absolute shrinkage and selection operator (LASSO), and multivariate Cox analyses were performed to construct a prognostic signature, which was evaluated using Kaplan–Meier survival and time-dependent receiver operating characteristic (ROC) analyses. Functional enrichment analyses Gene Ontology [GO], Kyoto Encyclopedia of Genes and Genomes [KEGG] and gene set enrichment analysis [GSEA], mutation profiling, tumor mutational burden, immune infiltration estimation, and consensus clustering were applied to characterize associated features. A key LRL was identified through integrated bioinformatic screening and prioritization. Its biological role was assessed by quantitative reverse transcription polymerase chain reactionq (RT-PCR), western blotting, BODIPY staining, colony formation, Transwell assays, and xenograft models. RNA sequencing followed by pathway enrichment analysis was conducted to explore underlying mechanisms. ***Results:*** A three-LRL signature (*AL031985.3*, *NRAV*, and *AC026412.3*) stratified HCC patients into distinct risk groups with significantly different survival outcomes and demonstrated independent prognostic value. *AC026412.3* was markedly upregulated in HCC and associated with poor prognosis. Functional assays demonstrated that *AC026412.3* promoted proliferation, invasion, and tumor growth while reducing lipid accumulation. Mechanistically, *AC026412.3* upregulated solute carrier family 22 member 5 (SLC22A5), enhanced fatty acid β-oxidation, and increased adenosine triphosphate (ATP) production, thereby driving metabolic reprogramming. ***Conclusions:*** This study establishes a robust LRL-based prognostic model and identifies *AC026412.3* as a key regulator of lipid metabolic reprogramming via the SLC22A5–fatty acid β-oxidation axis, highlighting its potential as a biomarker and therapeutic target in HCC.

Citation of this article: Liu L, Fan Y, Zou H, Hu S, Long K, Li L, *et al*. Lipid Metabolism-related lncRNA Model Identifies *AC026412.3* as a Driver of Fatty Acid β-oxidation in Hepatocellular Carcinoma. J Clin Transl Hepatol 2026. doi: 10.14218/JCTH.2026.00312.

Introduction

According to the latest Global Cancer Statistics, hepatocellular carcinoma (HCC) accounted for more than 900,000 newly diagnosed cases and over 830,000 deaths in 2020, underscoring its substantial global health burden.[1] Although advances in surgical resection, targeted therapy, and immunotherapy have improved the management of HCC, patient outcomes remain unsatisfactory because of pronounced molecular heterogeneity, frequent recurrence, and a strong tendency toward invasion and metastasis.[2]

The liver is highly susceptible to metabolic disturbances, and aberrant lipid homeostasis has been strongly implicated in the initiation and progression of HCC.[3,4] Accumulating evidence indicates that HCC cells frequently exhibit disrupted fatty acid synthesis, lipid oxidation, and cholesterol homeostasis. These alterations supply energy and biosynthetic precursors, foster an immunosuppressive microenvironment, and promote tumor growth, invasion, and immune evasion.[5]

Keywords: Hepatocellular carcinoma; HCC; Lipid metabolism; Long noncoding RNA; Prognostic model; fatty acid β-oxidation.

[#]Contributed equally to this work.

[*]**Correspondence to:** Qiang Kang, Department of Hepatopancreatobiliary Surgery, The Second Affiliated Hospital of Kunming Medical University, Kunming, Yunnan 650101, China. ORCID: https://orcid.org/0009-0004-7990-7541. Tel: +86-18313823750, Fax: +86-871-63402203, E-mail: kangqiang@kmmu.edu.cn; Zongqi Deng, The Second Affiliated Hospital of Kunming Medical University, Kunming, Yunnan 650101, China. ORCID: https://orcid.org/0009-0004-1126-0526. Tel: +86-18088345793, Fax: +86-871-65351281, E-mail: dengzongqi077@163.com.

Consequently, elucidating the molecular mechanisms underlying lipid metabolism dysregulation and leveraging them to develop molecular subtypes and prognostic models may provide new insights and therapeutic opportunities for personalized management of HCC.

Long noncoding RNAs (lncRNAs, >200 nt, non-protein-coding) regulate diverse cellular processes.[6–8] Recent evidence indicates that lncRNAs not only modulate gene transcription, chromatin remodeling, and signaling pathways but also play crucial roles in metabolic regulation and immune modulation in cancer.[9] Several lncRNAs have been shown to directly influence lipid metabolism and thereby drive HCC progression. For instance, small nucleolar RNA host gene 6 (*SNHG6*) promotes HCC development by coupling cholesterol sensing with mammalian target of rapamycin complex 1 (mTORC1) activation,[10] while downregulation of HNF4A antisense RNA 1 (*HNF4A-AS1*) facilitates resistance to sorafenib-induced ferroptosis through lipid metabolic reprogramming.[11] Nevertheless, comprehensive studies systematically investigating the prognostic value and molecular subtyping potential of lipid metabolism–related lncRNAs (LRLs) in HCC remain scarce, particularly those integrating clinical cohorts with experimental validation.

In this study, we systematically screened and identified LRLs using The Cancer Genome Atlas Liver Hepatocellular Carcinoma (TCGA-LIHC) cohort and subsequently constructed and validated a robust prognostic model. This model not only demonstrated strong predictive performance across multiple independent datasets but also uncovered distinct molecular subtypes characterized by differences in immune infiltration, somatic mutations, and drug sensitivity. Further functional analyses identified a previously unreported lncRNA, *AC026412.3*, which was markedly upregulated in HCC tissues and cell lines. Mechanistically, *AC026412.3* promoted HCC progression by enhancing fatty acid β-oxidation and adenosine triphosphate (ATP) production, thereby driving tumor cell proliferation and invasion. Collectively, our findings establish an LRL-based prognostic model for HCC and, for the first time, reveal the role of *AC026412.3* in promoting tumor progression through metabolic reprogramming. These results provide novel molecular insights into the metabolic heterogeneity of HCC and highlight potential biomarkers and therapeutic targets for prognostic assessment and precision therapy.

Methods

Public datasets and identification of LRLs

Transcriptome expression profiles and corresponding clinical information of 374 HCC patients were downloaded from the TCGA-LIHC database.[12] A total of 158 lipid metabolism–related genes were obtained from the HALLMARK_FATTY_ACID_METABOLISM gene set curated in the Molecular Signatures Database (Broad Institute; https://www.gsea-msigdb.org/gsea/msigdb/).[13] This gene set comprises genes involved in key biological processes related to fatty acid metabolism, including fatty acid transport, activation, β-oxidation, lipid utilization, and energy production (Supplementary Table 1). To identify LRLs, Pearson correlation analysis was performed between the expression profiles of lncRNAs and the 158 lipid metabolism–related genes.[14] lncRNAs with a correlation coefficient $|R| > 0.5$ and $P < 0.001$ were defined as LRLs. Subsequently, differentially expressed LRLs between HCC and normal liver tissues were identified using the limma package.[15] Patients were then randomly stratified into training and testing cohorts of equal size according to sex, age, and tumor node metastasis (TNM) stage for subsequent model construction and validation.

Construction and evaluation of the prognostic model

Prognostic LRLs were identified by univariate Cox regression in the training cohort, refined by least absolute shrinkage and selection operator (LASSO) regression, and incorporated into a multivariate Cox prognostic model.[16] Model performance was evaluated by Kaplan–Meier analysis and time-dependent receiver operating characteristic (ROC) curves across cohorts, and independent prognostic value was assessed by multivariable Cox regression adjusted for clinicopathological factors.[17]

Functional annotation, mutation profiling, immune landscape, and molecular subtyping

Risk-stratified differentially expressed genes were identified by limma ($|log2FC| > 1$, false discovery rate [FDR] < 0.05) and subjected to Gene Ontology (GO)/Kyoto Encyclopedia of Genes and Genomes (KEGG) enrichment analysis (clusterProfiler) and gene set enrichment analysis (GSEA) ($|$normalized enrichment score [NES]$| > 1$, FDR < 0.05).[15,18,19] Somatic mutations were profiled by maftools, with tumor mutational burden (TMB) calculated and assessed for prognostic interaction with the risk score.[20] Immune infiltration was estimated by Tumor Immune Estimation Resource (TIMER), Cell-type Identification By Estimating Relative Subsets Of RNA Transcripts (CIBERSORT), and Estimating the Proportions of Immune and Cancer (EPIC) cells, complemented by gene set variation analysis (GSVA)-based immune function scoring and checkpoint gene comparison.[21–24] Drug sensitivity was predicted by oncoPredict using the half-maximal inhibitory concentration (IC50).[25] Prognostic LRLs were used for consensus clustering (ConsensusClusterPlus), with subtype stability visualized by principal component analysis (PCA) and t-distributed stochastic neighbor embedding (t-SNE), and prognostic relevance evaluated by Kaplan–Meier analysis.[26,27]

Patients and tissue samples

Eighteen paired HCC tissues and matched adjacent non-tumorous liver tissues were collected from patients who underwent surgical resection at the Second Affiliated Hospital of Kunming Medical University from August 2024 to February 2025. None of the patients had received preoperative chemotherapy or radiotherapy. All diagnoses were independently confirmed by two experienced pathologists. Written informed consent was obtained from all participants before enrollment. This study was approved by the Ethics Committee of the Second Affiliated Hospital of Kunming Medical University on August 9, 2024 (Approval No. R-PJ-S-2024-125) before tissue collection and was conducted in accordance with the Declaration of Helsinki.

Cell culture

The normal human liver cell line transformed human liver epithelial-2 (THLE-2) and HCC cell lines HuH-7, HepG2, and Li-7 were obtained from Procell Life Science & Technology (Wuhan, China). THLE-2 cells were cultured in BEGM with fibronectin/collagen I/BSA precoating; HuH-7 and HepG2 cells were cultured in high-glucose DMEM; and Li-7 cells were cultured in RPMI-1640. All media contained 10% fetal bovine serum (FBS) and 1% penicillin-streptomycin.[4]

Plasmid construction, transfection, and establishment of stable cell lines

AC026412.3 was cloned into pcDNA3.1(+) for overexpression, and shRNAs targeting *AC026412.3*, negative regulator of antiviral response (*NRAV*), or *AL031985.3* were inserted

into pGPU6-GFP-Neo for knockdown. HCC cells were transfected with Lipofectamine 3000 and harvested at 48 h. For stable lines, lentiviral particles were generated and selected with puromycin (2 μg/mL, ~7 days).[8] Primer and shRNA sequences are provided in Supplementary Table 2.

Xenograft tumor assay

BALB/c nude mice (female, 4–6 weeks old, Kunming Medical University) were maintained under specific pathogen-free conditions. Experiments were approved by the Institutional Animal Care and Use Committee (Approval No. kmmu20211169). HuH-7 cells with stable *AC026412.3* overexpression, knockdown, or vector controls (1×10^6 cells in 100 μL Matrigel/Dulbecco's modified eagle medium (DMEM), 1:1) were subcutaneously injected into the right flank (n = 5 per group). Tumor volume was measured every 3–4 days using digital calipers and calculated as $(L \times W^2)/2$. Mice were euthanized at 4 weeks, and tumors were excised for weight measurement and lipid analysis.

RNA sequencing and bioinformatic analysis

Total RNA was extracted from *AC026412.3*-overexpressing and control HuH-7 cells (three replicates per group). mRNA libraries were prepared by poly(A) enrichment, fragmentation, cDNA synthesis, adapter ligation, and PCR amplification, then sequenced on an Illumina platform. Raw reads were processed by fastp, aligned to GRCh38.109 with HISAT2, and quantified by featureCounts. Differential expression was analyzed using DESeq2 ($|\log2FC| \geq 1$, FDR < 0.05).[28–31] The RNA-seq data generated in this study have been deposited in the Genome Sequence Archive (Genomics, Proteomics & Bioinformatics 2025) at the National Genomics Data Center (Nucleic Acids Research 2025), China National Center for Bioinformation/Beijing Institute of Genomics, Chinese Academy of Sciences (GSA-Human: HRA018230), and are publicly accessible at https://ngdc.cncb.ac.cn/gsa-human.[32,33]

Quantitative reverse transcription polymerase chain reaction (qRT-PCR) and Western blotting

qRT-PCR: Total RNA was extracted with TRIzol and reverse-transcribed using HiScript II Q RT SuperMix. qRT-PCR was performed with SYBR Green PCR Master Mix, with β-actin as the internal control.[7] Primer sequences are provided in Supplementary Table 3.

Western blotting: Protein lysates were prepared in radioimmunoprecipitation assay buffer with protease/phosphatase inhibitors, quantified by bicinchoninic acid assay, separated by sodium dodecyl sulfate–polyacrylamide gel electrophoresis, and transferred to polyvinylidene fluoride membranes. After blocking and antibody incubation, bands were visualized by enhanced chemiluminescence.[4] Antibody details are provided in Supplementary Table 4.

Cellular functional and lipid metabolic assays

Cell proliferation and invasion: Colony formation assays were performed with stably transfected cells seeded in 6-well plates and cultured for 2–3 weeks. Colonies were fixed, stained with crystal violet, and counted.[8] Cell invasion was assessed using Matrigel-coated Transwell chambers, with serum-free medium in the upper chamber and 10% FBS in the lower chamber as a chemoattractant. Invaded cells were fixed, stained, and quantified after 24 h.[7]

Lipid metabolism: Intracellular lipid droplets were visualized by BODIPY 493/503 staining (C2053, Beyotime Biotechnology, China) and confocal microscopy. Total cholesterol (E-BC-F032, Elabscience, China), triglyceride (E-BC-F033, Elabscience, China), and ATP levels (E-BC-F002, Elabscience, China) were measured by fluorometric/chemiluminescent assays, and fatty acid oxidation activity (E-BC-K784-M, Elabscience, China) was determined by colorimetric assay.

Statistical analysis

Statistical analyses were performed using R (v4.2.2).[34] Data are presented as mean ± SD. Group comparisons were assessed by Student's t-test or one-way ANOVA, and survival differences were analyzed by Kaplan–Meier analysis with a log-rank test. $P < 0.05$ was considered statistically significant.

Results

Identification of LRLs associated with HCC prognosis

The analytical workflow is summarized in Figure 1A. From TCGA-LIHC, 158 lipid metabolism–related genes yielded 962 correlated LRLs by Pearson analysis ($r > 0.5$, $P < 0.001$; Supplementary Table 5). Differential expression analysis identified 653 dysregulated LRLs in HCC versus adjacent normal tissues, visualized by volcano plot and heatmap (Fig. 1B and C). Univariate Cox regression in the training cohort identified 180 overall survival (OS)-associated LRLs, with hazard ratios shown in the forest plot and expression patterns shown in the heatmap (Fig. 1D and E).

Construction of an LRL-based prognostic model in HCC

LASSO regression refined the 180 candidate LRLs (Fig. 1F and G), and multivariate Cox analysis identified three independent prognostic indicators: *AL031985.3*, *NRAV*, and *AC026412.3*. The risk score formula was as follows: (0.696 × *AL031985.3*) + (0.415 × *NRAV*) + (1.643 × *AC026412.3*). Patients in the training, testing, and overall cohorts were stratified by the median risk score (Fig. 2A, F, and K), with survival status shown in Fig. 2B, G, and L and expression patterns shown in heatmaps (Fig. 2C, H, and M). High-risk patients exhibited significantly poorer OS (Fig. 2D, I, and N). Time-dependent ROC analysis demonstrated prognostic accuracy, with 1-/3-/5-year areas under the curve (AUCs) of 0.726/0.715/0.699 in the training set (Fig. 2E), 0.729/0.663/0.683 in the testing set (Fig. 2J), and 0.736/0.687/0.686 in the overall cohort (Fig. 2O).

Association of the LRL-based prognostic model with clinical factors

Multivariate Cox regression identified the LRL risk score as an independent prognostic factor for OS (HR 1.566, 95% CI 1.306–1.877, $P < 0.001$), whereas tumor stage was not independent of other variables (Fig. 3A and B). The risk score outperformed conventional clinical characteristics in predicting 5-year OS (Fig. 3C). Stratified analyses across age, sex, grade, and stage subgroups consistently showed poorer survival in high-risk patients (Fig. 3D–G), including a trend in the G3–4 subgroup despite limited statistical significance ($P = 0.115$; Fig. 3F).

Functional enrichment and genomic alterations in high- and low-risk subgroups

Differential expression analysis between high- and low-risk groups identified 1,597 upregulated and 107 downregulated genes (Fig. 4A and B). KEGG pathway enrichment analysis revealed that these differentially expressed genes were significantly associated with oncogenic signaling pathways, including the phosphatidylinositol 3-kinase-protein kinase

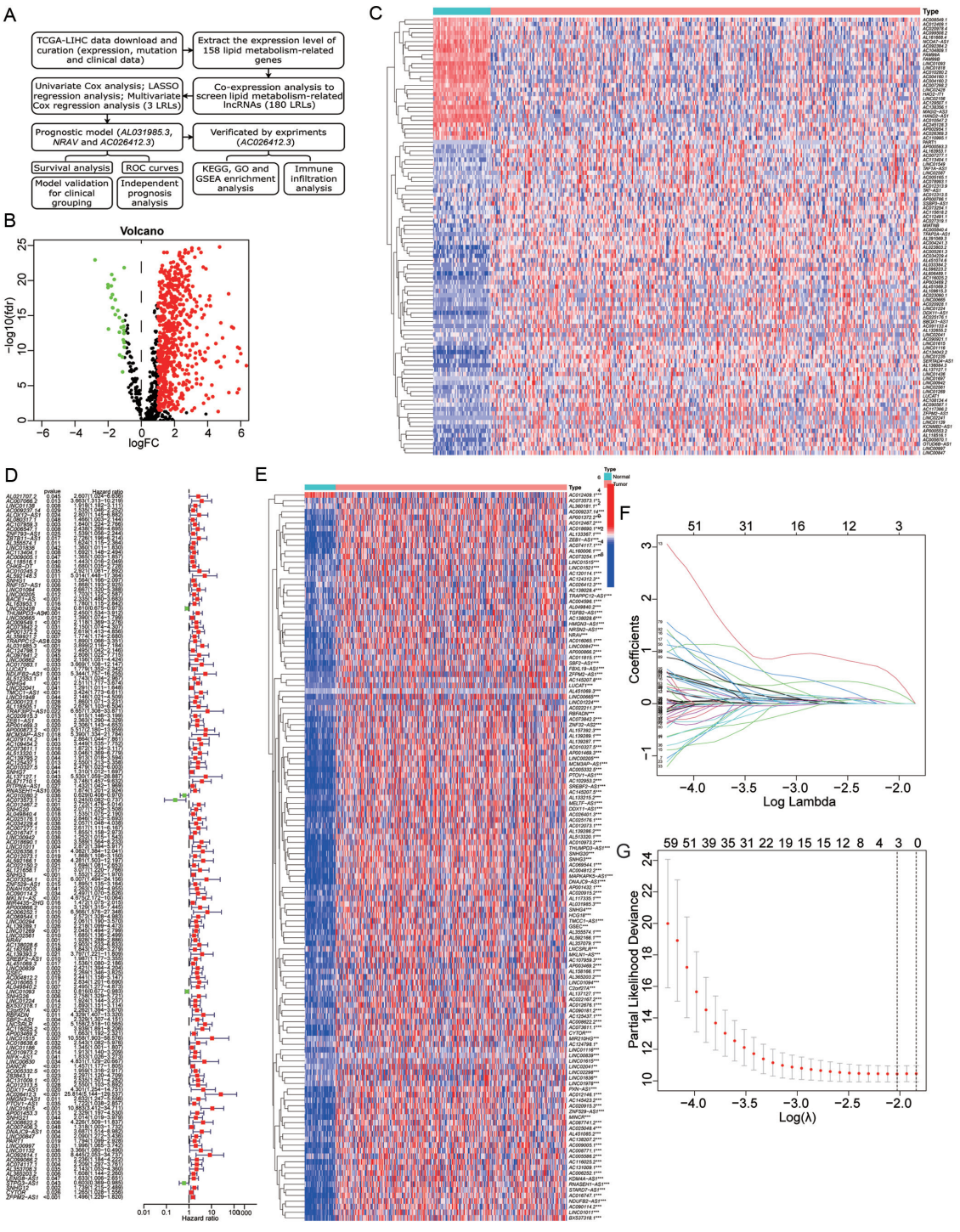

Fig. 1. Prognostic model and risk score based on LRLs in HCC. (A) Flowchart illustrating the complete bioinformatic workflow of this study. This includes the acquisition and preprocessing of TCGA-LIHC transcriptomic and clinical data, identification of lipid metabolism-related genes from MSigDB, Pearson correlation–based screening of LRLs, differential expression analysis, construction of the prognostic model using univariate Cox, LASSO, and multivariate Cox regression, followed by validation in training and testing cohorts, and downstream functional characterization, including enrichment analyses, immune infiltration evaluation, and experimental validation of key lncRNAs. (B) Volcano plot showing differentially expressed LRLs. (C) Heatmap displaying the expression patterns of the top 50 differentially expressed LRLs among the 653 identified LRLs in HCC samples. (D) Forest plot showing the hazard ratios and confidence intervals of 180 prognosis-related LRLs identified by univariate Cox regression analysis. (E) Heatmap illustrating the expression profiles of all 180 prognosis-related LRLs across HCC samples and their associations with clinical characteristics. (F) LASSO regression curve showing the shrinkage process of regression coefficients with varying log lambda values. (G) Partial likelihood deviance plot used to determine the optimal lambda value in LASSO regression for model construction. ***P < 0.001. HCC, hepatocellular carcinoma; TCGA-LIHC, The Cancer Genome Atlas Liver Hepatocellular Carcinoma; lncRNA, long noncoding RNA; LRLs, lipid metabolism-related lncRNAs; LASSO, least absolute shrinkage and selection operator; ROC, receiver operating characteristic; KEGG, Kyoto Encyclopedia of Genes and Genomes; GO, Gene Ontology; GSEA, gene set enrichment analysis.

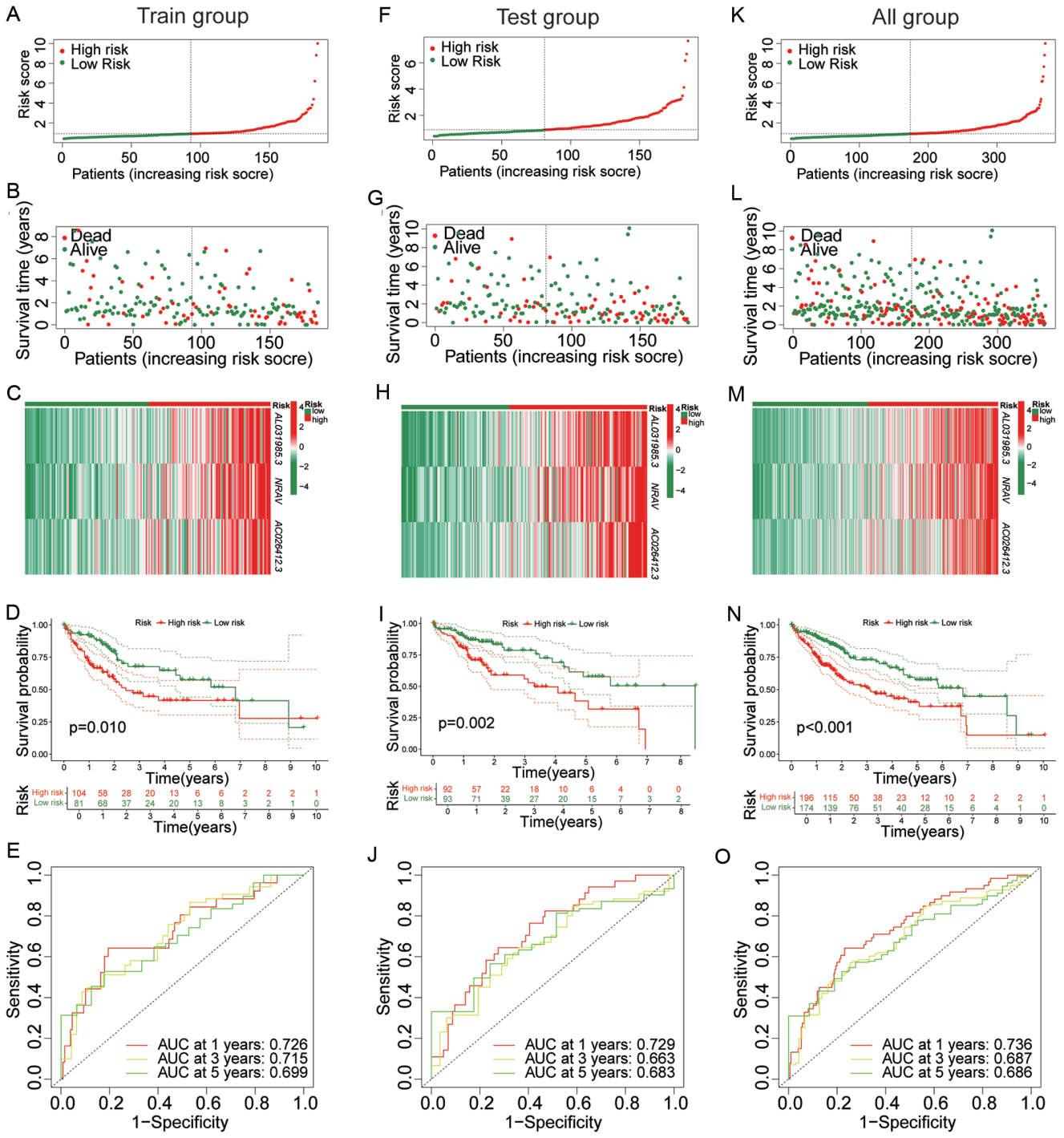

Fig. 2. Construction of the LRL-based prognostic model in HCC. (A, F, K) Distribution of risk scores in the training, testing, and overall cohorts, respectively, ranked from low to high. (B, G, L) Survival status and survival time of patients in the training, testing, and overall cohorts according to their risk scores. (C, H, M) Heatmaps showing the expression patterns of the prognostic LRLs between the high- and low-risk groups in the training, testing, and overall cohorts. (D, I, N) Kaplan–Meier survival curves comparing overall survival between the high- and low-risk groups in the training, testing, and overall cohorts. (E, J, O) Time-dependent ROC curves evaluating the predictive accuracy of the prognostic model for 1-, 3-, and 5-year overall survival in the training, testing, and overall cohorts. LRL, lipid metabolism-related lncRNA; HCC, hepatocellular carcinoma; ROC, receiver operating characteristic; AUC, area under the curve.

B (PI3K–Akt) signaling pathway (Fig. 4C). GO enrichment results were visualized using a bubble plot (Fig. 4D) and a Circos plot (Fig. 4E). In addition, GSEA demonstrated that cell cycle–related pathways were significantly enriched in the high-risk group, whereas fatty acid metabolism pathways were enriched in the low-risk group (Fig. 4F and G), suggesting a metabolic shift characterized by suppression of lipid metabolic programs and activation of proliferative signaling

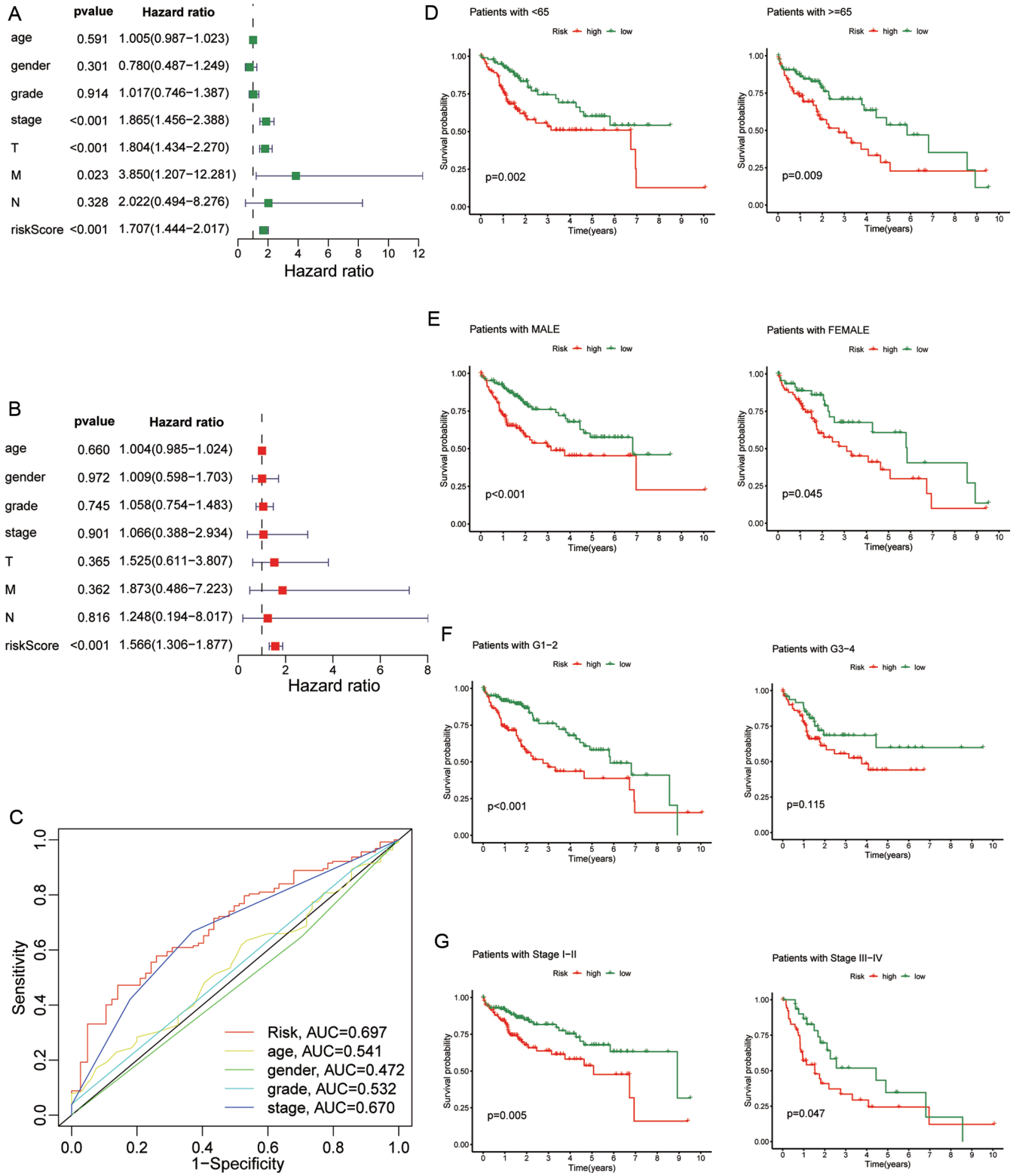

Fig. 3. Association of the LRL-based prognostic model with clinical features in HCC. (A–B) Univariate and multivariate Cox regression analyses of age, sex, grade, stage, and risk score in relation to overall survival. (C) Multivariate ROC curves comparing the predictive accuracy of the risk score and clinical characteristics (age, sex, grade, stage). (D–G) Kaplan–Meier survival curves stratified by clinical subgroups (age <65/≥65 (D), sex (E), grade G1–2/G3–4 (F), stage I–II/III–IV (G)), showing differences in overall survival between high- and low-risk groups. LRL, lipid metabolism-related lncRNA; HCC, hepatocellular carcinoma; ROC, receiver operating characteristic; AUC, area under the curve.

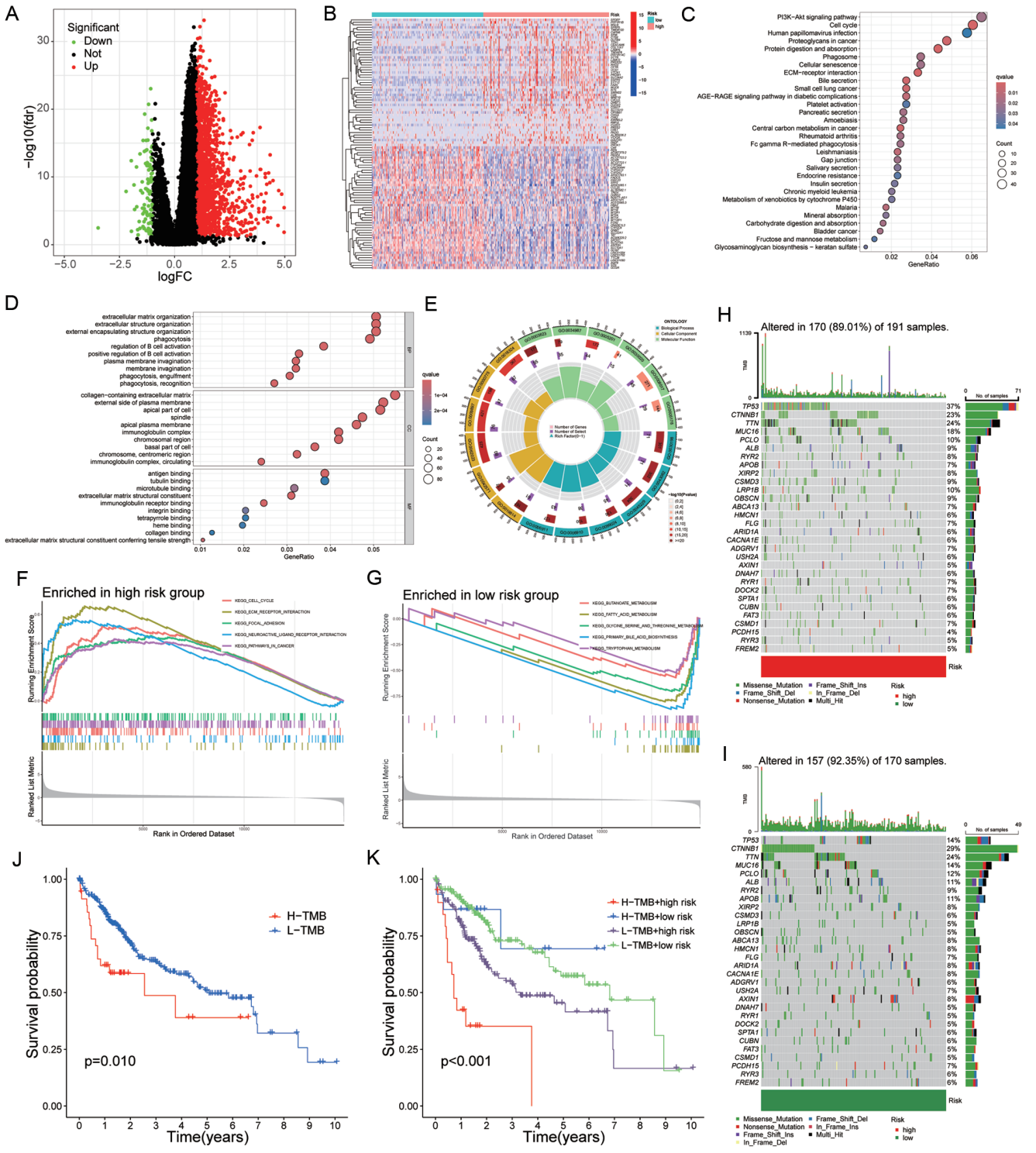

Fig. 4. Functional analysis of DEGs and mutation profiles between high- and low-risk groups. (A) Volcano plot showing DEGs between high- and low-risk groups. (B) Heatmap illustrating the expression patterns of DEGs in HCC samples. (C) KEGG pathway enrichment analysis of DEGs performed using clusterProfiler and presented as a bubble plot. Significantly enriched pathways were identified based on adjusted P values. (D) GO enrichment analysis of DEGs performed using clusterProfiler to systematically characterize functional alterations associated with risk stratification and presented as a bubble plot. (E) Circos plot displaying the distribution and regulation status of DEGs in GO pathways. (F) GSEA showing significantly enriched pathways in the high-risk group. (G) GSEA showing significantly enriched pathways in the low-risk group. (H, I) Waterfall plots illustrating somatic mutation profiles generated using maftools, visualizing mutational landscapes in high- and low-risk groups and highlighting differences in mutation frequency and the distribution of key driver genes. (J) Kaplan–Meier survival curves comparing overall survival between high-TMB and low-TMB groups. (K) Kaplan–Meier survival curves showing the combined prognostic impact of TMB and risk score. DEGs, differentially expressed genes; HCC, hepatocellular carcinoma; KEGG, Kyoto Encyclopedia of Genes and Genomes; GO, Gene Ontology; GSEA, gene set enrichment analysis; TMB, tumor mutational burden.

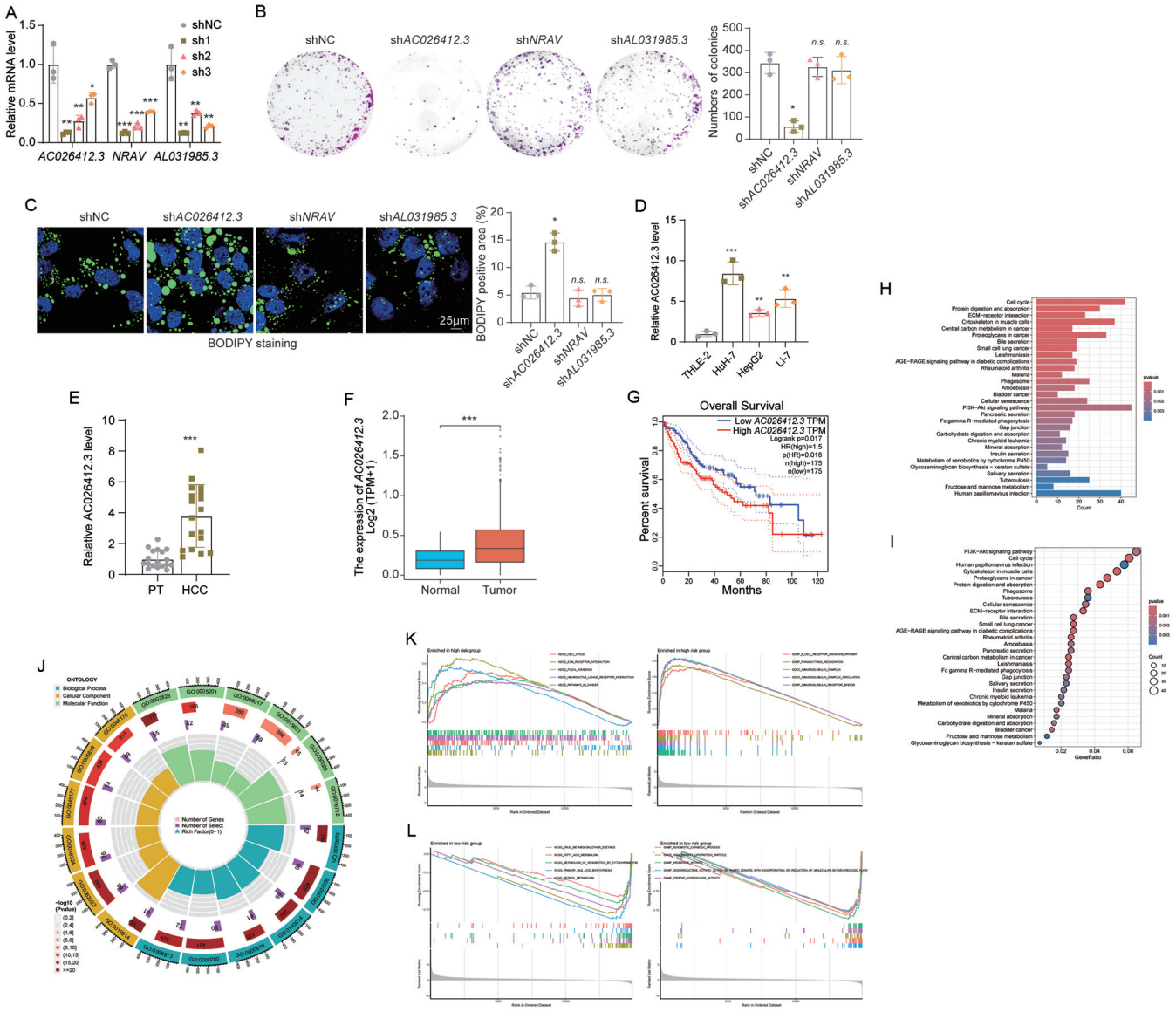

Fig. 5. Identification of *AC026412.3* as a key lipid metabolism–related lncRNA in HCC. (A) qRT-PCR analysis of lncRNA expression levels in HuH-7 cells transfected with shNC, sh*AC026412.3*, sh*NRAV*, or sh*AL031985.3* plasmids (n = 3 per group). (B) Colony formation assays showing the clonogenic growth ability of HuH-7 cells after transfection with shNC, sh*AC026412.3*, sh*NRAV*, or sh*AL031985.3* plasmids (n = 3 per group). (C) BODIPY staining showing lipid droplet accumulation in HuH-7 cells after transfection with shNC, sh*AC026412.3*, sh*NRAV*, or sh*AL031985.3* plasmids (n = 3 per group). Scale bar = 25 μm. (D) qRT-PCR analysis of *AC026412.3* expression in the normal human liver cell line THLE-2 and HCC cell lines HuH-7, HepG2, and Li-7 (n = 3 per group). (E) qRT-PCR analysis of *AC026412.3* expression in HCC tissues and matched adjacent non-tumorous tissues from 18 patients with HCC (n = 18 pairs). (F) *AC026412.3* expression in HCC tissues (n = 371) and normal liver samples (n = 160) from public datasets. (G) Kaplan–Meier survival curve showing the association between *AC026412.3* expression and overall survival in HCC patients (n = 350). (H) Bar plot showing KEGG pathway enrichment of *AC026412.3*-associated differentially expressed genes. (I) Bubble plot showing KEGG pathway enrichment of *AC026412.3*-associated differentially expressed genes. (J) Circos plot showing GO enrichment of *AC026412.3*-associated differentially expressed genes. (K) GSEA showing pathways enriched in the high-*AC026412.3*-expression group. (L) GSEA showing pathways enriched in the low-*AC026412.3*-expression group. Data are presented as mean ± SD. n.s., not significant; **P* < 0.05, ***P* < 0.01, ****P* < 0.001. HCC, hepatocellular carcinoma; lncRNA, long noncoding RNA; qRT-PCR, quantitative real-time polymerase chain reaction; BODIPY, boron-dipyrromethene; KEGG, Kyoto Encyclopedia of Genes and Genomes; GO, Gene Ontology; GSEA, gene set enrichment analysis; ECM, extracellular matrix; n.s., not significant.

in high-risk tumors.

Somatic mutation profiling revealed tumor protein p53 (TP53), catenin beta 1 (CTNNB1), and TTN as the most frequently mutated genes in the high-risk group, with the TP53 mutation rate markedly higher in high-risk (37%) versus low-risk (14%) patients (Fig. 4H and I). TMB stratification showed worse survival in high-TMB patients (Fig. 4J), and combined TMB–risk analysis demonstrated that high-TMB/high-risk patients had the poorest outcomes, with a synergistic effect exceeding that of either factor alone (Fig. 4K).

Identification of AC026412.3 as a key LRL in HCC

Among the three prognostic LRLs, *AC026412.3* emerged as the primary candidate for further functional validation. qRT-PCR confirmed the knockdown efficiency of *AC026412.3*, *NRAV*, and *AL031985.3* in HuH-7 cells (Fig. 5A). Colony for-

mation assays showed that *AC026412.3* knockdown markedly suppressed the clonogenic growth of HuH-7 cells, whereas *NRAV* or *AL031985.3* knockdown did not exert a comparable inhibitory effect (Fig. 5B). In addition, BODIPY staining demonstrated that *AC026412.3* knockdown substantially increased lipid droplet accumulation, while *NRAV* or *AL031985.3* silencing had no significant effect on lipid deposition (Fig. 5C). These results suggest that *AC026412.3* is the key LRL most closely associated with both malignant growth and lipid metabolic regulation in HCC.

AC026412.3 was significantly upregulated in HCC cell lines, including HuH-7, HepG2, and Li-7, compared with the normal human liver cell line THLE-2 (Fig. 5D). Consistently, *AC026412.3* expression was increased in 18 paired HCC tissues compared with matched adjacent non-tumorous tissues (Fig. 5E), and this upregulation was further confirmed in public datasets (Fig. 5F). Survival analysis from GEPIA showed that elevated *AC026412.3* expression was associated with poorer OS in HCC patients (Fig. 5G).

Functional enrichment analyses further indicated that *AC026412.3*-associated differentially expressed genes were involved in oncogenic signaling and metabolic reprogramming (Fig. 5H–J). GSEA showed that cell cycle, focal adhesion, and ECM–receptor interaction pathways were enriched in the high-*AC026412.3* expression group (Fig. 5K), whereas fatty acid metabolism, bile acid biosynthesis, and retinol metabolism pathways were enriched in the low-*AC026412.3* expression group (Fig. 5L). Collectively, these findings identify *AC026412.3* as a key LRL linking lipid dysregulation to aggressive HCC phenotypes.

AC026412.3 promotes lipid consumption and tumor progression in HCC

AC026412.3 overexpression in HuH-7 cells markedly decreased lipid droplet accumulation (Fig. 6A and B), contrasting with increased lipid deposition upon *AC026412.3* knockdown (Fig. 5C). Overexpression enhanced proliferation (Fig. 6C) and invasion (Fig. 6D), while subcutaneous xenografts showed larger tumors with reduced total cholesterol and triglyceride levels (Fig. 6E–I). Conversely, *AC026412.3* knockdown suppressed proliferation and invasion *in vitro* (Fig. 6J and K), reduced tumor weight and volume (Fig. 6L–N), and increased intracellular lipid content (Fig. 6O and P). These results indicate that *AC026412.3* drives HCC malignant progression by promoting lipid consumption.

AC026412.3 upregulates the lipid metabolism–related gene solute carrier family 22 member 5 (SLC22A5) in HCC

RNA-seq of *AC026412.3*-overexpressing HuH-7 cells showed 356 upregulated and 419 downregulated genes, with no batch effects (Fig. 7A and B). Pearson correlation identified six genes significantly correlated with *AC026412.3* ($r > 0.5$, $P < 0.001$), of which only *SLC22A5* was lipid metabolism–related (Fig. 7C). This finding was further supported by Spearman analysis in GEPIA ($R = 0.6$, $P < 0.0001$; Fig. 7E) and Pearson correlation analysis in 18 paired clinical samples ($R = 0.7481$, $P < 0.0001$; Fig. 7F), consistent with this correlation observed in the initial LRL screening (Supplementary Table 5). qRT-PCR and Western blot analyses collectively demonstrated the regulatory relationship: *AC026412.3* knockdown reduced SLC22A5 mRNA and protein levels, whereas overexpression increased both (Fig. 7G–J).

AC026412.3 promotes fatty acid β-oxidation and energy production in HCC

KEGG analysis of *AC026412.3*-overexpressing HuH-7 cells revealed activation of fatty acid β-oxidation-related pathways, including PPAR signaling and fatty acid degradation (Fig. 8A), with upregulation of key fatty acid β-oxidation genes *SLC22A5, CPT1A*, and *CPT2* (Fig. 8B). SLC22A5 facilitates carnitine transport for mitochondrial β-oxidation via the carnitine shuttle system (CPT1A, CACT, CPT2). Pearson correlation analysis in clinical samples confirmed positive correlations between *AC026412.3* and these shuttle components (Fig. 8C). *AC026412.3* knockdown reduced, whereas overexpression enhanced, their mRNA (Fig. 8D) and protein (Fig. 8E) levels. Functionally, *AC026412.3* silencing decreased fatty acid β-oxidation activity and intracellular ATP levels, whereas overexpression increased both (Fig. 8F and G). These findings demonstrate that *AC026412.3* promotes HCC progression by activating SLC22A5-mediated β-oxidation, thereby driving ATP-dependent metabolic reprogramming.

Immune landscape and therapeutic implications in high- and low-risk subgroups

Immune landscape and therapeutic implications of LRL-based stratification: Immune deconvolution revealed higher $CD4^+$ T-cell infiltration in the high-risk group, alongside reduced B cells, mast cells, natural killer (NK) cells, and T helper cells (Supplementary Fig. 1A). Functional enrichment showed suppressed cytolytic activity and interferon responses, indicating an immunosuppressive microenvironment (Supplementary Fig. 1B and C). Immune checkpoint genes were upregulated in high-risk patients (Supplementary Fig. 1D). Drug sensitivity prediction identified oxaliplatin, gemcitabine, and selumetinib as potentially effective in high-risk patients, with the opposite profile observed in low-risk patients (Supplementary Fig. 1E).

Molecular subtyping: Consensus clustering identified three robust subtypes (C1–C3, $k = 3$) with distinct risk distributions: C2 was primarily low-risk, C1 was enriched for high-risk patients, and C3 showed a balanced distribution (Supplementary Fig. 2A–E). C1 exhibited the poorest survival (Supplementary Fig. 2F), with PCA and t-SNE confirming subtype separation (Supplementary Fig. 2G and H).

Subtype-specific immune and therapeutic profiles: C3 showed the highest immune infiltration and Estimation of Stromal and Immune cells in Malignant Tumor tissues using Expression data (ESTIMATE) scores (Supplementary Fig. 3A and B), with distinct checkpoint expression patterns suggesting variable immunotherapy responses (Supplementary Fig. 3C). Drug sensitivity differed across subtypes: C1 showed sensitivity to oxaliplatin/axitinib, C2 to 5-fluorouracil/fulvestrant, and C3 to gallibiscoquinazole (Supplementary Fig. 3D). These findings indicate that LRL-based subtypes capture immune heterogeneity and may guide personalized therapy.

Discussion

HCC is one of the most lethal malignancies worldwide, with poor prognosis largely driven by molecular heterogeneity and high recurrence rates. Metabolic reprogramming is recognized as a hallmark of cancer,[35] and lipid-associated metabolic alterations represent a key feature of HCC cells.[36–38] Abnormal lipid metabolism not only provides energy and essential building blocks for tumor growth but also contributes to the establishment of an immunosuppressive microenvironment. lncRNAs have emerged as critical regulators of metabolic pathways, including fatty acid synthesis, fatty acid oxidation, and cholesterol homeostasis, and are increasingly recognized as potential biomarkers.[39,40] In this study, we developed a prognostic model based on LRLs and identified *AC026412.3* as a crucial driver of fatty acid β-oxidation and

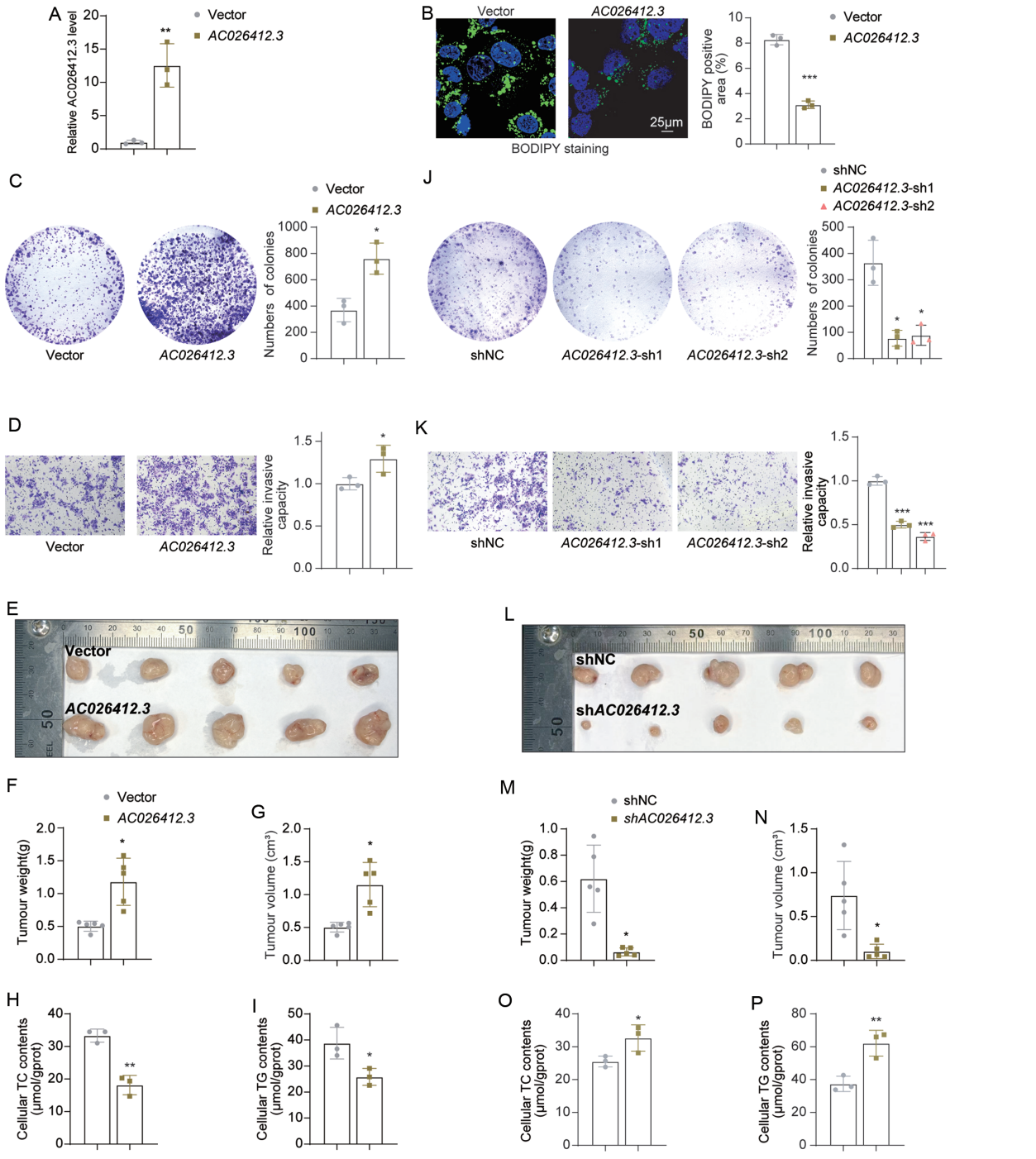

Fig. 6. Effects of *AC026412.3* on lipid accumulation, cell behavior, and tumor growth in HCC. (A) qRT-PCR analysis of *AC026412.3* expression in HuH-7 cells transfected with vector or *AC026412.3* overexpression plasmids (n = 3 per group). (B) BODIPY staining showing lipid droplet accumulation in HuH-7 cells transfected with vector or *AC026412.3* overexpression plasmids (n = 3 per group). Scale bar = 25 μm. (C–D) Colony formation and Transwell assays showing the proliferation and invasion abilities of HuH-7 cells transfected with vector or *AC026412.3* overexpression plasmids (n = 3 per group). (E) Representative images of xenograft tumors derived from HuH-7 cells transfected with vector or *AC026412.3* overexpression plasmids (n = 5 per group). (F–G) Quantification of tumor weight and tumor volume in xenograft models derived from HuH-7 cells transfected with vector or *AC026412.3* overexpression plasmids (n = 5 per group). (H–I) Measurement of TC and TG levels in xenograft tumor tissues derived from HuH-7 cells transfected with vector or *AC026412.3* overexpression plasmids (n = 3 per group, randomly selected from five tumors in each group). (J–K) Colony formation and Transwell assays showing the proliferation and invasion abilities of HuH-7 cells transfected with shNC or sh*AC026412.3* plasmids (n = 3 per group). (L) Representative images of xenograft tumors derived from HuH-7 cells transfected with shNC or sh*AC026412.3* plasmids (n = 5 per group). (M–N) Quantification of tumor weight and tumor volume in xenograft models derived from HuH-7 cells transfected with shNC or sh*AC026412.3* plasmids (n = 5 per group). (O–P) Measurement of TC and TG levels in xenograft tumor tissues derived from HuH-7 cells transfected with shNC or sh*AC026412.3* plasmids (n = 3 per group, randomly selected from five tumors in each group). Data are presented as mean ± SD. n.s., not significant; **P* < 0.05, ***P* < 0.01, ****P* < 0.001. HCC, hepatocellular carcinoma; qRT-PCR, quantitative real-time polymerase chain reaction; BODIPY, boron-dipyrromethene; TC, total cholesterol; TG, triglyceride.

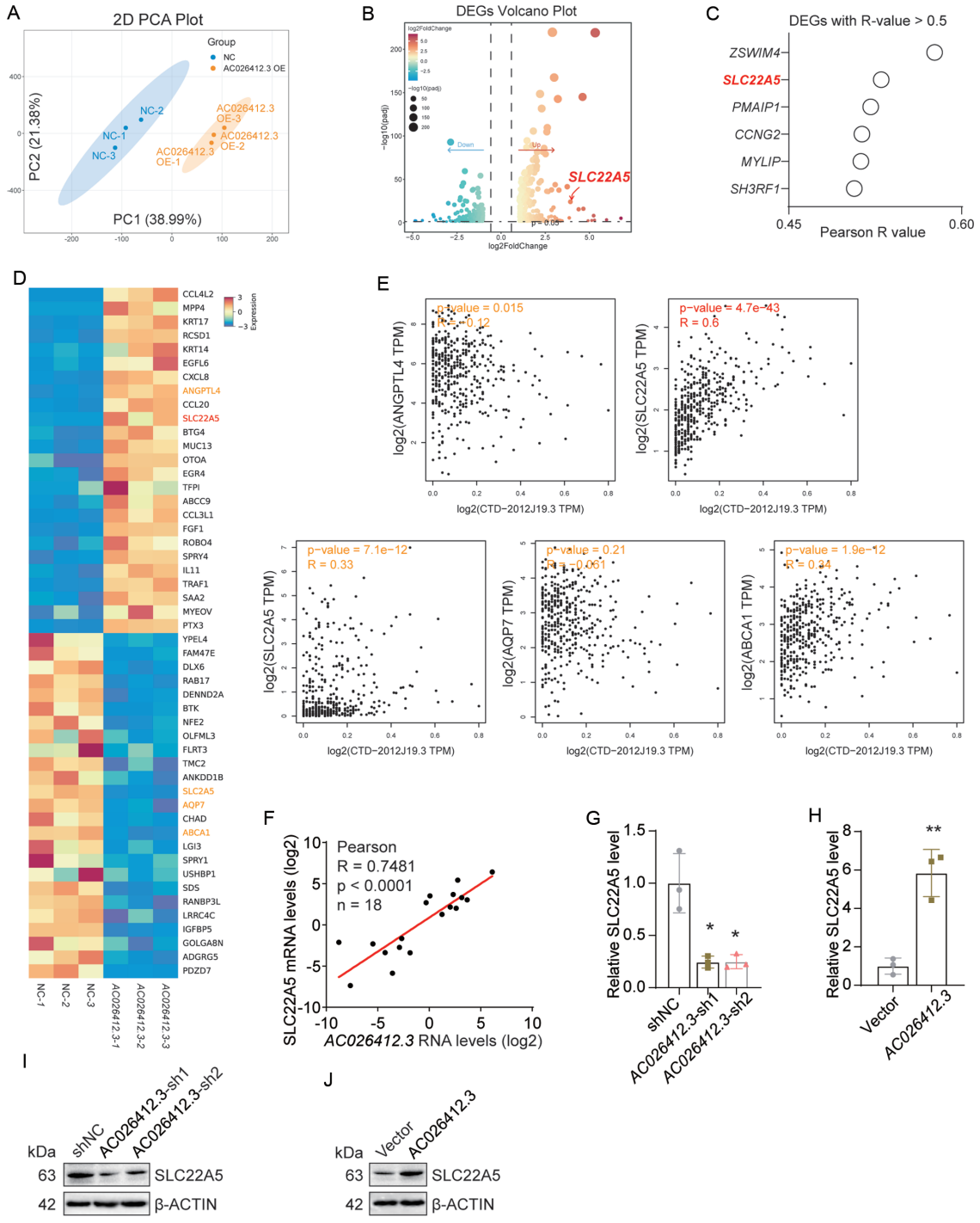

Fig. 7. Transcriptomic analysis and expression validation of candidate genes associated with *AC026412.3*. (A) PCA showing the clustering of transcriptomic profiles between HuH-7 cells overexpressing *AC026412.3* and control cells (n = 3 per group). (B) Volcano plot illustrating differentially expressed genes following *AC026412.3* overexpression (n = 3 per group). (C) Pearson correlation analysis identifying genes significantly correlated with *AC026412.3* expression (correlation coefficient > 0.5, $P < 0.001$). (D) Heatmap displaying the top 25 upregulated and top 25 downregulated genes following *AC026412.3* overexpression (n = 3 per group). (E) Spearman correlation analysis using the GEPIA platform showing the relationship between *AC026412.3* expression and candidate lipid metabolism-related genes (*ABCA1, AQP7, ANGPTL4, SLC2A5,* and *SLC22A5*) in HCC samples. (F) Pearson correlation analysis between *AC026412.3* and SLC22A5 mRNA expression in 18 paired HCC samples (n = 18). (G) qRT-PCR analysis of *SLC22A5* mRNA expression in HuH-7 cells transfected with shNC or sh*AC026412.3* plasmids (n = 3 per group). (H) qRT-PCR analysis of *SLC22A5* mRNA expression in HuH-7 cells transfected with vector or *AC026412.3* overexpression plasmids (n = 3 per group). (I) Western blot analysis of SLC22A5 protein levels in HuH-7 cells transfected with shNC or sh*AC026412.3* plasmids (three independent experiments). (J) Western blot analysis of SLC22A5 protein levels in HuH-7 cells transfected with vector or *AC026412.3* overexpression plasmids (three independent experiments). Data are presented as mean ± SD. n.s., not significant; **P* < 0.05, ***P* < 0.01. HCC, hepatocellular carcinoma; RNA-seq, RNA sequencing; PCA, principal component analysis; GEPIA, Gene Expression Profiling Interactive Analysis; qRT-PCR, quantitative real-time polymerase chain reaction; WB, western blotting.

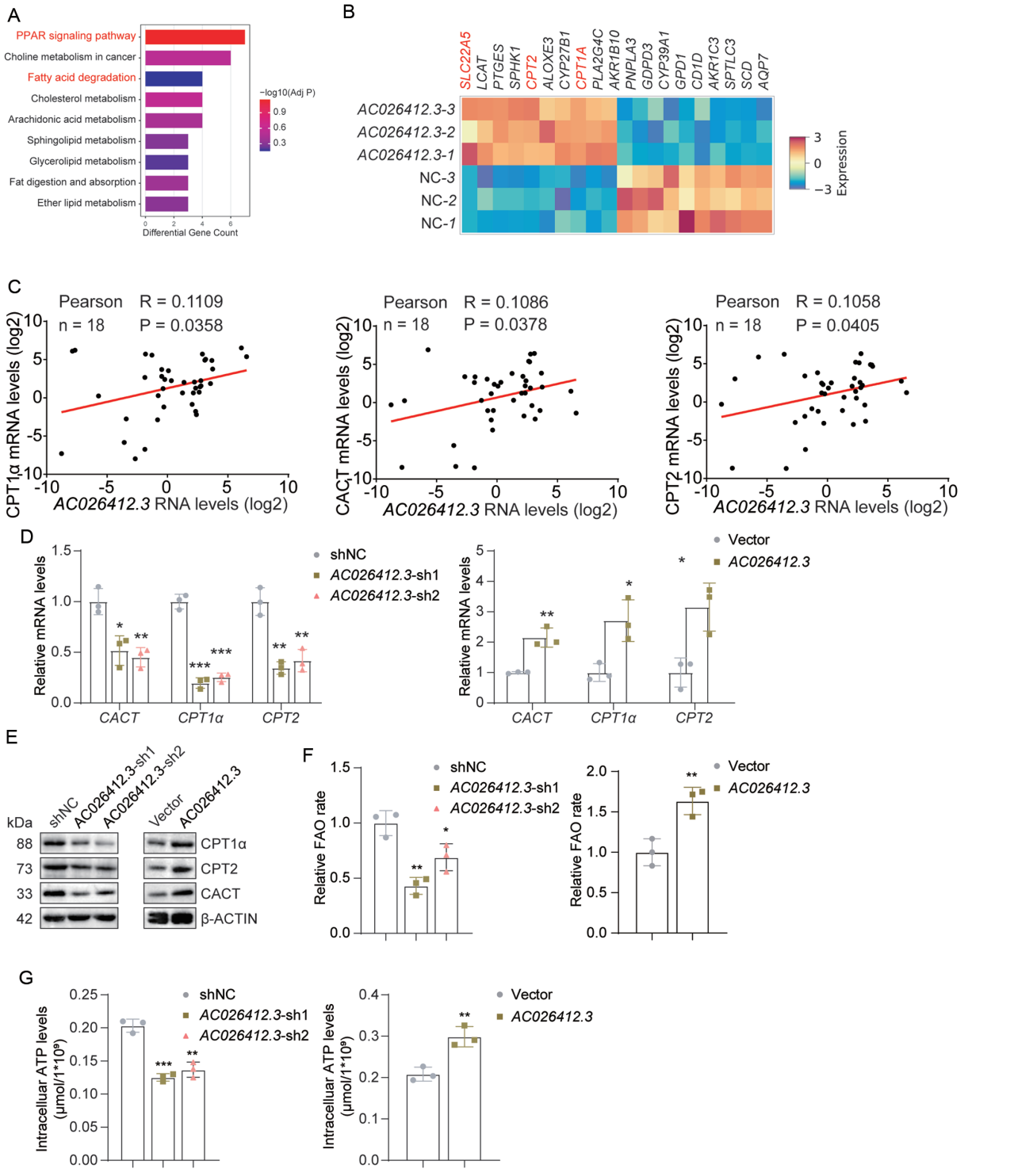

Fig. 8. Analysis of fatty acid β-oxidation and energy metabolism associated with *AC026412.3* in HCC. (A) KEGG pathway enrichment analysis of differentially expressed genes following *AC026412.3* overexpression (n = 3 per group). (B) Heatmap displaying differentially expressed lipid metabolism-related genes in HuH-7 cells after *AC026412.3* overexpression (n = 3 per group). (C) Pearson correlation analysis between *AC026412.3* expression and the mRNA levels of *CPT1A*, *CPT2,* and *CACT* in clinical HCC samples (n = 18). (D) qRT-PCR analysis of *CPT1A*, *CPT2*, and *CACT* mRNA expression in HuH-7 cells with *AC026412.3* overexpression or knockdown (n = 3 per group). (E) Western blot analysis of CPT1A, CPT2, and CACT protein levels in HuH-7 cells with *AC026412.3* overexpression or knockdown (three independent experiments). (F) Measurement of fatty acid β-oxidation activity in HuH-7 cells with *AC026412.3* overexpression or knockdown (n = 3 per group). (G) Measurement of intracellular ATP levels in HuH-7 cells with *AC026412.3* overexpression or knockdown (n = 3 per group). Data are presented as mean ± SD. n.s., not significant; **P* < 0.05, ***P* < 0.01, ****P* < 0.001. HCC, hepatocellular carcinoma; KEGG, Kyoto Encyclopedia of Genes and Genomes;fatty acid β-oxidation; PPAR, peroxisome proliferator-activated receptor; CACT, carnitine-acylcarnitine translocase; qRT-PCR, quantitative real-time polymerase chain reaction; ATP, adenosine triphosphate.

tumor progression in HCC.

Our model, composed of three LRLs *(AL031985.3*, *NRAV*, and *AC026412.3*), effectively stratified patients into distinct risk groups with significantly different survival outcomes. The risk score remained an independent prognostic factor when compared with conventional clinical features, and its predictive accuracy was confirmed in multiple subgroups. Although a growing number of HCC lncRNA prognostic signatures have been reported, including those related to metabolism, lipid metabolism, and cholesterol metabolism, most of these studies primarily function as correlative stratification tools focused on clinical outcome prediction, such as OS, recurrence risk, immune landscape, or immunotherapy response.[41,42] For example, Lei *et al*. developed a cholesterol metabolism–related lncRNA signature for prognostic and immunotherapy response prediction in HCC, representing a typical signature-level model based on statistical associations.[43] In contrast to previous correlation-based studies, our work integrates functional validation of a key lncRNA. Specifically, *AC026412.3* was identified as a novel LRL with confirmed biological relevance in HCC. Therefore, our study links prognostic modeling with functional characterization, providing a more biologically meaningful understanding of lipid metabolism–related heterogeneity in HCC.

Differential expression and enrichment analyses revealed that high-risk patients exhibited activation of cell cycle and PI3K–Akt signaling pathways, while low-risk patients were enriched in fatty acid metabolism. Notably, although these results appear to reflect a shift from metabolic pathways to proliferative signaling, this pattern represents a well-recognized feature of metabolic reprogramming in HCC, in which dysregulated lipid metabolism is tightly coupled with oncogenic signaling networks. Previous studies have demonstrated that PI3K/AKT/mammalian target of rapamycin (mTOR) signaling not only regulates tumor metabolism, including lipid metabolic processes, but also promotes lipogenesis and hepatocarcinogenesis through downstream effectors such as ribosomal protein S6 (RPS6).[44,45] Conversely, aberrant fatty acid metabolism in HCC is closely linked to Akt/mTOR/sterol regulatory element-binding protein 1c (SREBP1c)-mediated regulation of lipid-metabolizing enzymes.[46,47] Together, these findings support a bidirectional interplay between lipid metabolism and oncogenic signaling.

Mutation analysis further showed that TP53 alterations were more frequent in the high-risk group, consistent with its association with poor prognosis. Immune profiling demonstrated reduced immune cell infiltration and impaired interferon responses in high-risk tumors, suggesting an immunosuppressive phenotype. Consensus clustering further divided patients into three molecular subtypes with distinct prognoses, immune profiles, and therapeutic sensitivities. Importantly, subtype-specific immune checkpoint expression and drug sensitivity patterns suggest potential applications of the LRL signature in guiding immunotherapy and chemotherapy.

Functional validation demonstrated that *AC026412.3* promotes lipid utilization and enhances tumor aggressiveness. Mechanistically, *AC026412.3* upregulates SLC22A5 and fatty acid oxidation–related genes, including acyl-CoA oxidase 1 (ACOX1), carnitine palmitoyltransferase 1A (CPT1A), carnitine palmitoyltransferase 2 (CPT2), and carnitine-acylcarnitine translocase (CACT), thereby stimulating β-oxidation and ATP production. This finding extends the current understanding of lipid metabolism–associated lncRNAs in HCC. Previous studies have highlighted several representative regulatory axes. For example, *SNHG6* links cholesterol sensing to mTORC1 activation, thereby coupling lipid availability with oncogenic signaling pathways,[10] while *HNF4A-AS1* regulates lipid metabolic remodeling and contributes to sorafenib-induced ferroptosis resistance through lipid homeostasis control.[11] In addition, lncHR1 modulates lipid metabolism via the *SREBP-1c*–fatty acid synthase (FAS) axis, maintaining lipid synthesis under metabolic stress conditions.[48] Collectively, these lncRNAs primarily regulate cholesterol sensing, lipid biosynthesis, or ferroptosis-associated lipid remodeling, underscoring the diverse roles of lipid-related lncRNAs in HCC. In contrast, *AC026412.3* represents a distinct class of metabolic regulator that preferentially governs fatty acid utilization rather than lipid synthesis or cholesterol-centered signaling. In HCC, *AC026412.3* functions as a key metabolic driver linking SLC22A5-mediated carnitine transport to enhanced fatty acid β-oxidation, thereby reshaping lipid metabolism and promoting tumor progression. This finding not only underscores the central role of lipid metabolic reprogramming in HCC pathogenesis but also highlights the *AC026412.3*–SLC22A5–fatty acid β-oxidation axis as a potential therapeutic target.

From a translational perspective, our findings provide a comprehensive and clinically relevant framework for improving the management of HCC. First, the LRL signature demonstrates robust prognostic stratification beyond conventional clinicopathological parameters, enabling more precise identification of high-risk patients who may benefit from intensified surveillance, closer follow-up, and individualized therapeutic strategies. This suggests its potential utility as a clinically implementable molecular tool, such as a qRT-PCR–based panel, to complement existing staging systems and improve risk-adapted decision-making in HCC. Second, the integration of immune infiltration profiles, somatic mutation landscapes, TMB, and drug sensitivity predictions further extends its translational relevance by providing a multidimensional framework for therapeutic stratification, which may assist in selecting patients more likely to respond to specific systemic therapies, including targeted therapy and immunotherapy. Third, and most importantly, functional validation of *AC026412.3* identifies a previously unrecognized metabolic vulnerability in HCC, defined by the *AC026412.3*–SLC22A5–fatty acid β-oxidation axis. Given the central role of fatty acid oxidation in sustaining ATP production and tumor growth, this pathway represents a potentially druggable metabolic dependency, offering opportunities for therapeutic intervention targeting lipid utilization or carnitine transport–dependent metabolism.

Several limitations should be acknowledged. First, the clinical validation cohort consisted of only 18 paired HCC and adjacent non-tumorous tissues, which may limit the generalizability and translational applicability of our findings. Therefore, larger independent multicenter cohorts and prospective clinical studies are required to further validate the prognostic value and clinical utility of *AC026412.3*. Second, the precise molecular mechanism by which *AC026412.3* regulates SLC22A5 and fatty acid β-oxidation remains to be fully elucidated. Third, drug sensitivity results were derived from computational predictions and thus require experimental confirmation. Future research should integrate transcriptomic, metabolomic, and proteomic approaches to comprehensively delineate the role of LRLs in HCC. Therapeutic strategies targeting *AC026412.3*-mediated fatty acid β-oxidation may open new avenues for precision medicine in this malignancy.

Conclusions

We developed an LRL signature that effectively predicts prognosis and stratifies HCC patients into clinically and biologically distinct groups. This model demonstrated independent

prognostic value and provided insights into immune infiltration, mutational profiles, and therapeutic responses. Further functional studies identified *AC026412.3* as a key oncogenic lncRNA that promotes fatty acid β-oxidation and ATP production, thereby driving tumor growth and invasion. These findings highlight the importance of LRLs in HCC progression and suggest that targeting *AC026412.3* or its downstream metabolic pathways may offer novel opportunities for precision prognostication and therapy.

Supporting information

Supplementary material for this article is available at https://doi.org/10.14218/JCTH.2026.00312.

Funding

This study was supported by the Yunnan Health Training Project of High-Level Talents (H-2025048), the Scientific Research Fund Project of the Yunnan Provincial Department of Education (2025J325 and 2026J0224), and the Yunnan Fundamental Research Kunming Medical University Joint Projects (202601AY070001-246).

Conflict of interest

The authors have no conflict of interests related to this publication.

Author contributions

Study concept and design (LxL, YF, ZD, QK), acquisition of data (LxL, YF, HZ, SH, KL, LhL, CX, HW, YL, RF), analysis and interpretation of data (LxL, YF, HZ, CX, ZD, QK), drafting of the manuscript (LxL, YF), critical revision of the manuscript for important intellectual content (CX, ZD, QK), administrative, technical, or material support (SH, KL, LhL, HW, YL, RF), and study supervision (ZD, QK). All authors have made significant contributions to this study and have approved the final manuscript.

Ethical statement

This study was approved by the Ethics Committee of the Second Affiliated Hospital of Kunming Medical University on August 9, 2024 (Approval No. R-PJ-S-2024-125) before tissue collection and was conducted in accordance with the Declaration of Helsinki (as revised in 2024). Written informed consent was obtained from all patients prior to tissue collection. All animal experiments were approved by the Institutional Animal Care and Use Committee of Kunming Medical University (Approval No. kmmu20211169) and were conducted in accordance with institutional guidelines for animal care and use. All animals received humane care

Data sharing statement

The datasets analyzed in this study are publicly available from The Cancer Genome Atlas (TCGA) database (https://portal.gdc.cancer.gov/). The RNA-seq data generated during the current study have been deposited in the Genome Sequence Archive (Genomics, Proteomics & Bioinformatics 2025) in the National Genomics Data Center (Nucleic Acids Res 2025), China National Center for Bioinformation/Beijing Institute of Genomics, Chinese Academy of Sciences (GSA-Human: HRA018230), and are publicly accessible at https://ngdc.cncb.ac.cn/gsa-human.

References

[1] Rumgay H, Arnold M, Ferlay J, Lesi O, Cabasag CJ, Vignat J, *et al*. Global burden of primary liver cancer in 2020 and predictions to 2040. J Hepatol 2022;77(6):1598–1606. doi:10.1016/j.jhep.2022.08.021, PMID:36208844.
[2] Brown ZJ, Tsilimigras DI, Ruff SM, Mohseni A, Kamel IR, Cloyd JM, *et al*. Management of Hepatocellular Carcinoma: A Review. JAMA Surg 2023;158(4):410–420. doi:10.1001/jamasurg.2022.7989, PMID:36790767.
[3] Sharpton SR, Loomba R. Emerging role of statin therapy in the prevention and management of cirrhosis, portal hypertension, and HCC. Hepatology 2023;78(6):1896–1906. doi:10.1097/HEP.0000000000000278, PMID:37013380.
[4] Xia C, Zhang X, Li J, Xu N, Hu S, Lu Q, *et al*. OCTN2 Activates a Non-Canonical Carnitine Metabolic Pathway to Promote MASH-HCC Progression and Immunotherapy Resistance. Adv Sci (Weinh) 2026;13(16):e17054. doi:10.1002/advs.202517054, PMID:41566533.
[5] Cao LQ, Xie Y, Fleishman JS, Liu X, Chen ZS. Hepatocellular carcinoma and lipid metabolism: Novel targets and therapeutic strategies. Cancer Lett 2024;597:217061. doi:10.1016/j.canlet.2024.217061, PMID:38876384.
[6] Li Y, He Y, Han S, Liang Y. Identification and Functional Inference for Tumor-Associated Long Non-Coding RNA. IEEE/ACM Trans Comput Biol Bioinform 2019;16(4):1288–1301. doi:10.1109/TCBB.2017.2687442, PMID:28358691.
[7] Li Y, Xia C, Li J, Qin J, Shi F, Zhang W, *et al*. NK cell-associated long non-coding RNAs reveal heterogeneity of colorectal cancer immune microenvironment. Front Immunol 2025;16:1615942. doi:10.3389/fimmu.2025.1615942, PMID:41322425.
[8] Li J, Xia C, Li Y, Liu H, Gong C, Liang D. Effects of NK cell-related lncRNA on the immune microenvironment and molecular subtyping for pancreatic ductal adenocarcinoma. Front Immunol 2024;15:1514259. doi:10.3389/fimmu.2024.1514259, PMID:39872533.
[9] Herman AB, Tsitsipatis D, Gorospe M. Integrated lncRNA function upon genomic and epigenomic regulation. Mol Cell 2022;82(12):2252–2266. doi:10.1016/j.molcel.2022.05.027, PMID:35714586.
[10] Liu F, Tian T, Zhang Z, Xie S, Yang J, Zhu L, *et al*. Long non-coding RNA SNHG6 couples cholesterol sensing with mTORC1 activation in hepatocellular carcinoma. Nat Metab 2022;4(8):1022–1040. doi:10.1038/s42255-022-00616-7, PMID:35995997.
[11] Zhao Y, Han S, Zeng Z, Zheng H, Li Y, Wang F, *et al*. Decreased lncRNA HNF4A-AS1 facilitates resistance to sorafenib-induced ferroptosis of hepatocellular carcinoma by reprogramming lipid metabolism. Theranostics 2024;14(18):7088–7110. doi:10.7150/thno.99197, PMID:39629121.
[12] Cancer Genome Atlas Research Network. Comprehensive and Integrative Genomic Characterization of Hepatocellular Carcinoma. Cell 2017;169(7):1327–1341.e23. doi:10.1016/j.cell.2017.05.046, PMID:28622513.
[13] Liberzon A, Birger C, Thorvaldsdóttir H, Ghandi M, Mesirov JP, Tamayo P. The Molecular Signatures Database (MSigDB) hallmark gene set collection. Cell Syst 2015;1(6):417–425. doi:10.1016/j.cels.2015.12.004, PMID:26771021.
[14] Pearson K. Mathematical contributions to the theory of evolution.-On a form of spurious correlation which may arise when indices are used in the measurement of organs. Proc R Soc Lond 1897;60(359-367):489–498. doi:10.1098/rspl.1896.0076.
[15] Ritchie ME, Phipson B, Wu D, Hu Y, Law CW, Shi W, *et al*. limma powers differential expression analyses for RNA-sequencing and microarray studies. Nucleic Acids Res 2015;43(7):e47. doi:10.1093/nar/gkv007, PMID:25605792.
[16] Friedman J, Hastie T, Tibshirani R. Regularization Paths for Generalized Linear Models via Coordinate Descent. J Stat Softw 2010;33(1):1–22. PMID:20808728.
[17] Blanche P, Dartigues JF, Jacqmin-Gadda H. Estimating and comparing time-dependent areas under receiver operating characteristic curves for censored event times with competing risks. Stat Med 2013;32(30):5381–5397. doi:10.1002/sim.5958, PMID:24027076.
[18] Subramanian A, Tamayo P, Mootha VK, Mukherjee S, Ebert BL, Gillette MA, *et al*. Gene set enrichment analysis: a knowledge-based approach for interpreting genome-wide expression profiles. Proc Natl Acad Sci U S A 2005;102(43):15545–15550. doi:10.1073/pnas.0506580102, PMID:16199517.
[19] Yu G, Wang LG, Han Y, He QY. clusterProfiler: an R package for comparing biological themes among gene clusters. OMICS 2012;16(5):284–287. doi:10.1089/omi.2011.0118, PMID:22455463.
[20] Mayakonda A, Lin DC, Assenov Y, Plass C, Koeffler HP. Maftools: efficient and comprehensive analysis of somatic variants in cancer. Genome Res 2018;28(11):1747–1756. doi:10.1101/gr.239244.118, PMID:30341162.
[21] Li T, Fan J, Wang B, Traugh N, Chen Q, Liu JS, *et al*. TIMER: A Web Server for Comprehensive Analysis of Tumor-Infiltrating Immune Cells. Cancer Res 2017;77(21):e108–e110. doi:10.1158/0008-5472.CAN-17-0307, PMID:29092952.
[22] Newman AM, Liu CL, Green MR, Gentles AJ, Feng W, Xu Y, *et al*. Robust enumeration of cell subsets from tissue expression profiles. Nat Methods 2015;12(5):453–457. doi:10.1038/nmeth.3337, PMID:25822800.
[23] Racle J, de Jonge K, Baumgaertner P, Speiser DE, Gfeller D. Simultaneous enumeration of cancer and immune cell types from bulk tumor gene expression data. Elife 2017;6:e26476. doi:10.7554/eLife.26476, PMID:29130882.
[24] Hänzelmann S, Castelo R, Guinney J. GSVA: gene set variation analysis for microarray and RNA-seq data. BMC Bioinformatics 2013;14:7. doi:10.1186/1471-2105-14-7, PMID:23323831.

[25] Maeser D, Gruener RF, Huang RS. oncoPredict: an R package for predicting in vivo or cancer patient drug response and biomarkers from cell line screening data. Brief Bioinform 2021;22(6):bbab260. doi:10.1093/bib/bbab260, PMID:34260682.
[26] Wilkerson MD, Hayes DN. ConsensusClusterPlus: a class discovery tool with confidence assessments and item tracking. Bioinformatics 2010;26(12):1572–1573. doi:10.1093/bioinformatics/btq170, PMID:20427518.
[27] Laurens VDM, Hinton G. Visualizing Data using t-SNE. J Mach Learn Res 2008;9(2605):2579–2605.
[28] Chen S, Zhou Y, Chen Y, Gu J. fastp: an ultra-fast all-in-one FASTQ preprocessor. Bioinformatics 2018;34(17):i884–i890. doi:10.1093/bioinformatics/bty560, PMID:30423086.
[29] Kim D, Paggi JM, Park C, Bennett C, Salzberg SL. Graph-based genome alignment and genotyping with HISAT2 and HISAT-genotype. Nat Biotechnol 2019;37(8):907–915. doi:10.1038/s41587-019-0201-4, PMID:31375807.
[30] Liao Y, Smyth GK, Shi W. featureCounts: an efficient general purpose program for assigning sequence reads to genomic features. Bioinformatics 2014;30(7):923–930. doi:10.1093/bioinformatics/btt656, PMID:24227677.
[31] Love MI, Huber W, Anders S. Moderated estimation of fold change and dispersion for RNA-seq data with DESeq2. Genome Biol 2014;15(12):550. doi:10.1186/s13059-014-0550-8, PMID:25516281.
[32] Zhang S, Chen X, Jin E, Wang A, Chen T, Zhang X, *et al*. The GSA Family in 2025: A Broadened Sharing Platform for Multi-omics and Multimodal Data. Genomics Proteomics Bioinformatics 2025;23(4):qzaf072. doi:10.1093/gpbjnl/qzaf072, PMID:40857552.
[33] CNCB–NGDC Members and Partners. Database resources of the National Genomics Data Center, China National Center for Bioinformation in 2026. Nucleic Acids Res 2026;54(D1):D28–D47. doi:10.1093/nar/gkaf1172, PMID:41359036.
[34] The R Core Team. R: A Language and Environment for Statistical Computing. Vienna, Austria: R Foundation for Statistical Computing. 2010;14:12-21.
[35] Du X, Wan S, Chen Y, Qu P, Huang X, Yu X, *et al*. Genetic variants in genes of tricarboxylic acid cycle key enzymes predict postsurgical overall survival of patients with hepatocellular carcinoma. Ann Surg Oncol 2014;21(13):4300–4307. doi:10.1245/s10434-014-3876-2, PMID:25081338.
[36] Peng C, Kaščáková S, Chiappini F, Olaya N, Sandt C, Yousef I, *et al*. Discrimination of cirrhotic nodules, dysplastic lesions and hepatocellular carcinoma by their vibrational signature. J Transl Med 2016;14:9. doi:10.1186/s12967-016-0763-6, PMID:26754490.
[37] Soukupova J, Malfettone A, Hyroššová P, Hernández-Alvarez MI, Peñuelas-Haro I, Bertran E, *et al*. Role of the Transforming Growth Factor-β in regulating hepatocellular carcinoma oxidative metabolism. Sci Rep 2017;7(1):12486. doi:10.1038/s41598-017-12837-y, PMID:28970582.
[38] Skill NJ, Scott RE, Wu J, Maluccio MA. Hepatocellular carcinoma associated lipid metabolism reprogramming. J Surg Res 2011;169(1):51–56. doi:10.1016/j.jss.2009.09.005, PMID:19932908.
[39] Wu LL, Cai WP, Lei X, Shi KQ, Lin XY, Shi L. NRAL mediates cisplatin resistance in hepatocellular carcinoma via miR-340-5p/Nrf2 axis. J Cell Commun Signal 2019;13(1):99–112. doi:10.1007/s12079-018-0479-x, PMID:30030687.
[40] Huang H, Bu YZ, Zhang XY, Liu J, Zhu LY, Fang Y. LINC01433 promotes hepatocellular carcinoma progression via modulating the miR-1301/STAT3 axis. J Cell Physiol 2019;234(5):6116–6124. doi:10.1002/jcp.27366, PMID:30317567.
[41] Li W, Chen QF, Huang T, Wu P, Shen L, Huang ZL. Identification and Validation of a Prognostic lncRNA Signature for Hepatocellular Carcinoma. Front Oncol 2020;10:780. doi:10.3389/fonc.2020.00780, PMID:32587825.
[42] Wang X, Qian J, Yao N, Pocha C, Kang KJ, Angelico R, *et al*. Identification of metabolism-related long non-coding RNA (lncRNA) signature predicts prognosis and immune infiltrates in hepatocellular carcinoma. Ann Transl Med 2022;10(10):595. doi:10.21037/atm-22-2194, PMID:35722420.
[43] Lei H, Xiang T, Zhu H, Hu X. A Novel Cholesterol Metabolism-Related lncRNA Signature Predicts the Prognosis of Patients with Hepatocellular Carcinoma and Their Response to Immunotherapy. Front Biosci (Landmark Ed) 2024;29(3):129. doi:10.31083/j.fbl2903129, PMID:38538256.
[44] Tian LY, Smit DJ, Jücker M. The Role of PI3K/AKT/mTOR Signaling in Hepatocellular Carcinoma Metabolism. Int J Mol Sci 2023;24(3):2652. doi:10.3390/ijms24032652, PMID:36768977.
[45] Calvisi DF, Wang C, Ho C, Ladu S, Lee SA, Mattu S, *et al*. Increased lipogenesis, induced by AKT-mTORC1-RPS6 signaling, promotes development of human hepatocellular carcinoma. Gastroenterology 2011;140(3):1071–1083. doi:10.1053/j.gastro.2010.12.006, PMID:21147110.
[46] Wang M, Han J, Xing H, Zhang H, Li Z, Liang L, *et al*. Dysregulated fatty acid metabolism in hepatocellular carcinoma. Hepat Oncol 2016;3(4):241–251. doi:10.2217/hep-2016-0012, PMID:30191046.
[47] Li J, Huang Q, Long X, Zhang J, Huang X, Aa J, *et al*. CD147 reprograms fatty acid metabolism in hepatocellular carcinoma cells through Akt/mTOR/SREBP1c and P38/PPARα pathways. J Hepatol 2015;63(6):1378–1389. doi:10.1016/j.jhep.2015.07.039, PMID:26282231.
[48] Li D, Cheng M, Niu Y, Chi X, Liu X, Fan J, *et al*. Identification of a novel human long non-coding RNA that regulates hepatic lipid metabolism by inhibiting SREBP-1c. Int J Biol Sci 2017;13(3):349–357. doi:10.7150/ijbs.16635, PMID:28367099.